Size and boundary scattering controlled contribution of spectral phonons to the thermal conductivity in graphene ribbons

Yulu Shen,[1] Guofeng Xie,[1,a)] Xiaolin Wei,[1] Kaiwang Zhang,[1] Minghua Tang,[1] Jianxin Zhong,[1] Gang Zhang,[2,a)] and Yong-Wei Zhang[2]
[1]*Hunan Key Laboratory of Micro-Nano Energy Materials and Devices, Faculty of Materials, Optoelectronics and Physics, Xiangtan University, Hunan 411105, People's Republic of China*
[2]*Institute of High Performance Computing, Singapore 138632, Singapore*

(Received 16 October 2013; accepted 1 February 2014; published online 12 February 2014)

Although graphene holds great promise in thermal applications owing to its superior thermal conductivity, an intriguing question remains as to which polarizations and frequencies are dominant in its heat conduction. In this work, by incorporating the direction-dependent phonon-boundary scattering and the special selection rule for three-phonon scattering into the linearized phonon Boltzmann transport equation, we systematically investigate the relative contributions from longitudinal-acoustic, transverse-acoustic, and out-of-plane acoustic (ZA) branches to the thermal conductivity of graphene ribbons, focusing on the effects of their size and temperature. We find that the relative contribution from ZA branch to heat conduction increases with decreasing the size, specularity parameter, and temperature of graphene ribbons. Our analysis reveals that this change arises from the huge difference in the phonon dispersion and in the phonon mean free path of Umklapp process between in-plane and out-of-plane branches. © *2014 AIP Publishing LLC*.
[http://dx.doi.org/10.1063/1.4865744]

I. INTRODUCTION

The thermal transport of graphene has attracted a great deal of experimental[1–6] and theoretical[7–14] research interest. It is well-known that there are six phonon polarization branches in single layer graphene (SLG):[15–17] (i) out-of-plane acoustic (ZA) and out-of-plane optical phonons (ZO) with the displacement vector along the Z axis perpendicular to the graphene plane; (ii) transverse-acoustic (TA) and transverse-optical (TO) phonons, which correspond to the transverse vibrations within the graphene plane; and (iii) longitudinal-acoustic (LA) and longitudinal-optical (LO) phonons, which correspond to the longitudinal vibrations within the graphene plane. In general, the numbers of phonons in the optical branches (LO, TO, ZO) are at least an order-of-magnitude smaller than those in the acoustic branches over the entire temperature range. Combining with the low group velocities, it has been widely recognized that the contributions from the optical phonon branches to the thermal conductivity are much less than those from the acoustic branches.[15,16,18]

However, the relative contribution to heat conduction by LA, TA or ZA phonons is still an intriguing question in phonon transport of SLG.[19,20] Due to the small phonon group velocity, it was suggested that ZA phonons have a negligible contribution to the thermal conductivity of SLG.[15] A similar conclusion was also reached based on the calculation of thermal conductivity using linearized Boltzmann transport equation (BTE) within relaxation time approximation (RTA).[7,16,21–23] Wang *et al.*[3] suggested that the flexural phonon modes contributed significantly to the thermal transport of the suspended graphene since the experimentally measured temperature dependence of thermal conductivity of SLG followed a power law with an exponent of 1.4 ± 0.1. Through the full quantum mechanical calculations of both normal and Umklapp three-phonon scattering processes, Lindsay *et al.*[6,24] obtained a selection rule for three-phonon scattering, which strongly restricts the phase space for Umklapp scattering of ZA phonons in SLG. By incorporating this selection rule in the linearized phonon BTE for SLG, they found that the ZA modes could contribute as much as 77% and 86% of the total thermal conductivity at 300 K and 100 K, respectively. This result was based on the large density of flexural phonons associated with the quadratic ZA branch dispersion and the reflection symmetry of ideal two-dimensional graphene, thus significantly restricting the phase space for phonon-phonon scattering of the flexural modes.

Although the relative contributions to the thermal conductivity of SLG by different phonon branches were studied, the effects of graphene ribbon size, boundary roughness, and temperature on the thermal conductivity are still open questions. In this work, by introducing the direction-dependent phonon-boundary scattering to the linearized phonon Boltzmann transport equation, we investigate the effects of size and temperature on the thermal conductivity of graphene ribbons, as well as on the relative contributions by LA, TA and ZA branches in graphene ribbons. Different from literatures 7, 8, 15, and 21–23, the present model employs a frequency dependent Grüneisen parameter for the ZA branch. In addition, in calculating the scattering rate of Umklapp phonon-phonon process of flexural phonons, the present model includes a selection rule that any three-phonon scattering process in SLG must involve either no out-of-plane

a)Authors to whom correspondence should be addressed. Electronic addresses: gfxie@xtu.edu.cn and zhangg@ihpc.a-star.edu.sg

phonons or two out-of-plane phonons.[6,24] Our calculations reveal that the relative contribution of ZA branch to the heat conduction increases with decreasing the size, specularity parameter, and temperature. Importantly, the contribution of ZA mode should not be neglected (over 20%) in graphene ribbons with small size (less than 1 μm) and rough boundary (small specularity parameter less than 0.5), and at temperature lower than 50 K, the contribution of ZA even becomes dominant.

II. THEORETICAL MODEL AND DERIVATION

Here, we formulate our theoretical model of the thermal conductivity in graphene ribbons, which takes into account the anharmonic three-phonon processes, together with the direction-dependent phonon scattering from the ribbon edges (see the schematic illustration of phonon scattering processes in Fig. 1). According to linearized phonon BTE within RTA, the thermal conductivity in branch λ of graphene in the y direction (the longitudinal direction of graphene ribbon) is derived as

$$\kappa_\lambda = \frac{S}{(2\pi)^2}\int c_{ph} v_{\lambda,y}^2 \tau_\lambda d\vec{q} = \frac{S}{(2\pi)^2}\int_0^{q_{\max}}\int_0^{2\pi} \frac{k_B}{S\delta}\frac{(\hbar\omega/k_BT)^2 e^{\hbar\omega/k_BT}}{(e^{\hbar\omega/k_BT}-1)^2} v_\lambda^2 \cos^2\theta \tau_\lambda q d\theta dq, \quad (1)$$

where $\lambda = LA$, TA, and ZA, and only acoustic branches are considered.[15,18] S is the area of the sample, $v_{\lambda,y}$ is the y component of the group-velocity vector in branch λ, τ_λ is the averaged phonon relaxation time between successive scattering events of branch λ, $\vec{q}$ is the wave vector, θ (ranging from 0 to 2π) is the angle between the wave vector and y axis, and c_{ph} is the volumetric specific heat of each mode, which is given as

$$c_{ph} = \frac{k_B}{S\delta}\frac{(\hbar w/k_BT)^2 e^{\hbar w/k_BT}}{(e^{\hbar w/k_BT}-1)^2}, \quad (2)$$

where k_B is the Boltzmann constant, $\delta = 0.35$ nm is the thickness of graphene, $\hbar$ is the reduced Planck constant, and T is the absolute temperature.

In SLG, the LA and TA acoustic branches are linear, whereas the ZA branch shows a quadratic dependence of the frequency on the wave vector,[15,16] so

$$\omega_\lambda = \begin{cases} v_\lambda q & \lambda = LA,\ TA \\ \alpha q^2 & \lambda = ZA. \end{cases} \quad (3)$$

Using this dispersion and the relationship $v_\lambda = \frac{d\omega_\lambda}{dq}$, and transforming the integral of wave vector (q) to frequency (ω), we can get

$$\kappa_\lambda = \begin{cases} \frac{k_B}{4\pi^2\delta}\int_0^{\omega_{D,\lambda}}\int_0^{2\pi} \frac{(\hbar\omega/k_BT)^2 e^{\hbar\omega/k_BT}}{(e^{\hbar\omega/k_BT}-1)^2}\omega\cos^2\theta\tau_\lambda(\omega,\theta)d\theta d\omega & \lambda = LA,\ TA \\ \frac{k_B}{2\pi^2\delta}\int_0^{\omega_{D,\lambda}}\int_0^{2\pi} \frac{(\hbar\omega/k_BT)^2 e^{\hbar\omega/k_BT}}{(e^{\hbar\omega/k_BT}-1)^2}\omega\cos^2\theta\tau_\lambda(\omega,\theta)d\theta d\omega & \lambda = ZA, \end{cases} \quad (4)$$

where $\omega_{D,\lambda}$ is the Debye frequency, which is given as

$$\omega_{D,\lambda} = \begin{cases} 2v_\lambda\sqrt{\frac{\pi}{\Omega}} & \lambda = LA, TA \\ \frac{4\pi\alpha}{\Omega} & \lambda = ZA, \end{cases} \quad (5)$$

where Ω is the primitive cell area.

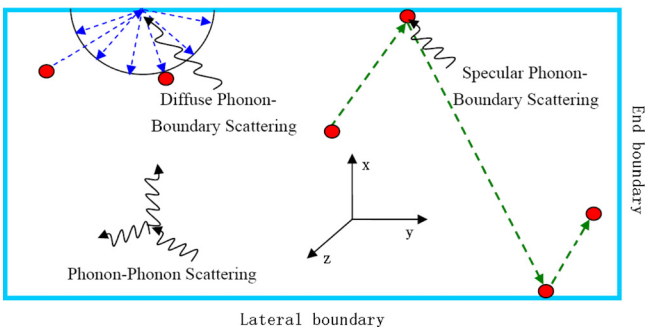

FIG. 1. Schematic illustration of phonon scattering processes in graphene ribbon.

According to Eq. (4), the expression of the averaged phonon relaxation time τ is the determinant of thermal conductivity value in graphene ribbon. The Matthiessen's rule, which assumes that different scattering mechanisms are independent, is applied to combine the effects of Umklapp phonon-phonon scattering (τ_U) and phonon-boundary scattering (τ_B). In the present work, we do not consider other scattering mechanisms such as defects, therefore $\tau^{-1} = \tau_U^{-1} + \tau_B^{-1}$. Based on the time-dependent perturbation theory, Roufosse and Klemens[25] derived the scattering rate for three-phonon processes. The relaxation time of Umklapp phonon-phonon scattering was derived using an expression from Refs. 22 and 26 but introducing separate lifetimes for LA, TA, and ZA phonons,

$$\tau_{U,\lambda} = \frac{M v_\lambda^2 \omega_{D,\lambda}}{\gamma_\lambda^2 k_B T \omega^2} e^{\Theta_\lambda/3T}, \quad (6)$$

where M is the mass of a graphene unit cell, γ_λ is the Grüneissen parameter, which controls the strength of the phonon-phonon scattering process for each branch, and Θ_λ is

the Debye temperature for each branch. The proper treatment of phonon-boundary scattering rate is critical in nanoscale system, especially when the characteristic size of the system is close to or less than the phonon mean free path. Here, we introduce the direction-dependent averaged relaxation time of phonon-boundary scattering $\tau_B(\theta)$, and according to the Matthiessen's rule, the averaged phonon relaxation time is derived as

$$\tau_\lambda(\omega,\theta) = \frac{\tau_{U,\lambda}(\omega)\tau_{B,\lambda}(\theta)}{\tau_{U,\lambda}(\omega)+\tau_{B,\lambda}(\theta)}. \tag{7}$$

As shown in Fig. 1, the phonon-boundary scattering in graphene ribbons includes end boundaries scattering and lateral boundaries scattering. For a rectangular graphene ribbon, the averaged relaxation time of phonon-boundary scattering τ_B is given as

$$\tau_{B,\lambda}(\theta,\xi) = \begin{cases} l_l/v_\lambda & \text{if } l_l < l_e \text{ and } \xi > P \\ l_e/v_\lambda & \text{if } l_l \geq l_e \text{ or } \xi \leq P, \end{cases} \tag{8}$$

where l_e is the averaged distance traveled ballistically by a phonon before hitting the end boundary, and l_l is the averaged distance traveled ballistically by a phonon before hitting the lateral boundary. P is the specularity parameter, which is defined as the probability of phonon's specular reflection at the lateral boundaries, and ξ is a random number ranging from 0 to 1. If $\xi \leq P$, the phonon boundary scattering is specular, otherwise the scattering is diffuse. The specular reflections of phonons at lateral boundaries mean that all phonons scatter at the boundary elastically preserving their momentum along the length. Such scattering events do not contribute to the thermal resistance of the sample. Therefore for the phonons along the propagation direction (θ) that are reflected specularly at the lateral boundaries, the averaged relaxation time of boundary scattering should be derived as l_e/v_λ, instead of l_l/v_λ, even though the scattering takes place at the lateral boundaries. Based on the assumption that the spatial distribution of phonons in the rectangular ribbon is uniform, l_e and l_l are given as follows:

$$l_e(\theta) = \frac{1}{L|\cos\theta|}\int_0^L y dy = \frac{L}{2|\cos\theta|}, \tag{9}$$

$$l_l(\theta) = \frac{1}{W|\sin\theta|}\int_0^W x dx = \frac{W}{2|\sin\theta|}, \tag{10}$$

where L is the length of the graphene ribbon, and W is the width of the ribbon. With this improved method, which allows for the calculation of the direction dependent phonon-boundary scattering rate, we can explore not only width dependence but also length dependence of thermal conductivity of graphene ribbons.

The parameters for dispersion originate from Ref. 27, the group velocity for *LA* and *TA* branches is 15 045 m/s and 10 640 m/s, respectively, and $\alpha = 4.09 \times 10^{-7}\,\mathrm{m^2/s}$ for *ZA* branch. The Grüneissen parameter for *LA* and *TA* is 2.0 and 1.0, respectively.[7] Unlike the LA and TA branches, the Grüneissen parameter for the ZA branch (γ_{ZA}) has a very strong dependence on wavevector,[16,17] and the range of $\gamma_{ZA}(q)$ is from −53 to −1.46, which is calculated by the first principles in Ref. 16. The shape of $\gamma_{ZA}(q)$ curve of single layer graphene in Ref. 16 is like quadratic, therefore we take the simple assumption,

$$\gamma_{ZA}(q) = -1.46 - \frac{51.54}{q_{\max}^2}(q-q_{\max})^2. \tag{11}$$

Substituting the quadratic dispersion of ZA phonons $\omega = \alpha q^2$ in Eq. (11), the frequency-dependence of the Grüneissen parameter $\gamma_{ZA}(\omega)$ is obtained. This simple assumption is more reliable than the approximated constant of γ_{ZA} in earlier reported works due to the strong wavevector (or frequency)-dependence of γ_{ZA}.

For a flat graphene sheet lying in the x-y plane, the reflection symmetry requires that the Hamiltonian be invariant under $z \to -z$.[6] Seol *et al.* obtained a selection rule for three-phonon scattering, which requires that an even number of ZA phonons is involved in each process. There are 12 processes in which ZA phonons are involved, according the selection rule, only the following 4 processes can occur: $ZA + ZA \leftrightarrow LA$, $ZA + ZA \leftrightarrow TA$, $LA + ZA \leftrightarrow ZA$, and $TA + ZA \leftrightarrow ZA$. The processes in which any odd number of ZA branches involved are forbidden, such as $ZA + ZA \leftrightarrow ZA$, $ZA + LA \leftrightarrow TA$, $LA + TA \leftrightarrow ZA$. Therefore, in our model, the scattering rate of Umklapp phonon-phonon process of flexural phonons is simply multiplied by a factor 1/3, and the relaxation time of Umklapp phonon-phonon scattering in Eq. (6) for ZA branch is modified as

$$\tau_{U,ZA}(\omega) = \frac{M v_{ZA}^2(\omega)\omega_{D,ZA}}{\gamma_{ZA}^2(\omega)k_B T\omega^2} e^{\Theta_{ZA}/3T} \times 3. \tag{12}$$

Lindsay *et al.* found that about 60% of both the N-process and U-process three-phonon scattering phase space of ZA phonons are forbidden by the selection rule,[24] which is consistent with our analysis.

Based on these derivations, now we can calculate the thermal conductivity of each branch and the total thermal conductivity, which is the sum of these three acoustic branches. The integral calculation of the thermal conductivity in graphene according to Eq. (4) cannot be carried out analytically, but it can be performed by Monte Carlo sampling method,[28] which is given as

$$\kappa_\lambda = \begin{cases} \dfrac{k_B\omega_{D,\lambda}}{2\pi\delta}\cdot\dfrac{1}{N}\displaystyle\sum_{i=1}^{N} g_\lambda(\omega_i,\theta_i,\xi_i) & \lambda = LA, TA \\ \dfrac{k_B\omega_{D,\lambda}}{\pi\delta}\cdot\dfrac{1}{N}\displaystyle\sum_{i=1}^{N} g_\lambda(\omega_i,\theta_i,\xi_i) & \lambda = ZA, \end{cases} \tag{13}$$

where N is the sampling number, and must be very large (for example, $N = 10^6$) in order to improve the accuracy and reduce the variance. $g_\lambda(\omega,\theta,\xi)$ is the integral function, which is expressed as

$$g_\lambda(\omega,\theta,\xi) = \frac{(\hbar\omega/k_B T)^2 e^{\hbar\omega/k_B T}}{(e^{\hbar\omega/k_B T}-1)^2}\omega\cos^2\theta\tau_\lambda(\omega,\theta,\xi). \tag{14}$$

ω, θ, and ξ are uniform distribution in the range of $[0, \omega_{D,\lambda}]$, $[0, 2\pi]$, and [0,1], respectively.

III. RESULTS AND DISCUSSIONS

We apply this model to investigate the effects of size, boundary, and temperature on the thermal conductivity of rectangular graphene ribbons. Fig. 2 shows the length dependence of total thermal conductivity in graphene ribbons with different specularity parameters ($0 \leq P \leq 1$). The width of the ribbons is 5 μm, and the temperature is 300 K. It is obvious that the probability of specular reflection at lateral boundaries has dominant influence on the length dependence of thermal conductivity in graphene ribbons. At a short length, the phonons with the mean free path (MFP) are limited by the length only, and thermal conductivity rapidly increases with length. Due to the large phonon MFP in 2D graphene, which is estimated to be of the order of 800 nm near room temperature,[2] the specularity parameter has little influence on the thermal conductivity of graphene ribbons with a short length. A further increase in length increases the number of phonons that experience lateral boundary scattering, resulting in MFP being dependent on both end and lateral boundary scattering, therefore the specularity parameter has increasing influence on the thermal conductivity as the length of the ribbon increases. The increasing slope of the thermal conductivity versus length curve is also related to the specularity parameter P: it decreases as the value of P decreases in the same length regime. The finite value of thermal conductivity results from the existence of diffuse phonon-boundary scattering. With the specularity parameter (P) decreases, the fraction of the diffusively scattered phonons increases, leading to a reduction in thermal conductivity. Our calculations are in good agreement with various experimental measurements which are plotted as scattering points in Fig. 2, circles taken from Ref. 1, square taken from Ref. 2 and rhomb taken from Ref. 4.

The length dependence of intrinsic thermal conductivity ($P = 1$, purely specular boundary reflection) of individual branch in graphene ribbons at room temperature is presented in Fig. 3(a). The intrinsic thermal conductivity of LA and TA branch has linear relationship with $\log L$ (where L is the length of the ribbon), which is in consistent with the results of Ref. 8, but the intrinsic thermal conductivity of ZA branch converges with L. In LA and TA branches, the anharmonic three-phonon scattering of the first-order alone is not sufficient for obtaining the normal diffusion in graphene ribbons, resulting in a divergent thermal conductivity. For convergent thermal conductivity in graphene ribbons, other scattering mechanisms must be included, such as diffuse boundary scattering, multiple phonon processes, and crystal lattice imperfections. The difference in the length dependence of thermal conductivity between the in-plane branches (LA and TA) and out-of-plane branch (ZA) stems from the different phonon dispersion.

A fundamental understanding of the relaxation time of phonons is essential to identify the influence of size on the thermal conductivity of graphene ribbons. The averaged relaxation time of phonons with different propagating directions in individual branch is derived as

$$\tau_\lambda(\omega) = \frac{\sum \tau_\lambda(\omega,\theta)}{2\pi} = \frac{1}{2\pi}\int_0^{2\pi} \frac{\tau_{U,\lambda}(\omega)\tau_{B,\lambda}(\theta)}{\tau_{U,\lambda}(\omega)+\tau_{B,\lambda}(\theta)} d\theta. \quad (15)$$

Fig. 3(b) gives the frequency dependence of averaged relaxation time of LA, TA, and ZA phonons in graphene ribbons

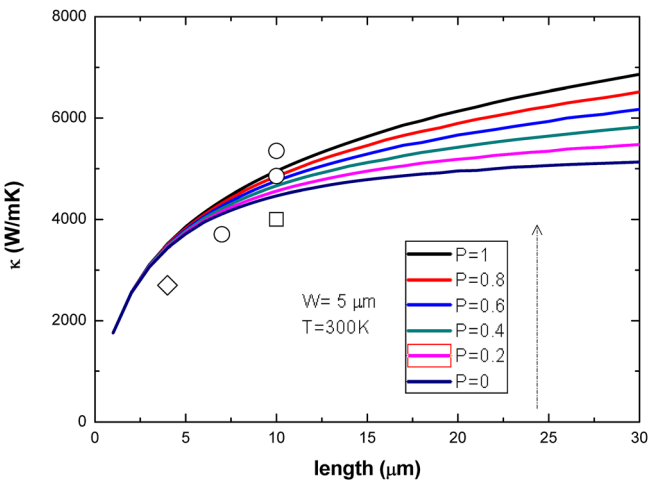

FIG. 2. The length dependence of thermal conductivity of graphene ribbons with different specularity parameters. Experimental data points from Ref. 1 (○), Ref. 2 (□), and Ref. 4 (◇).

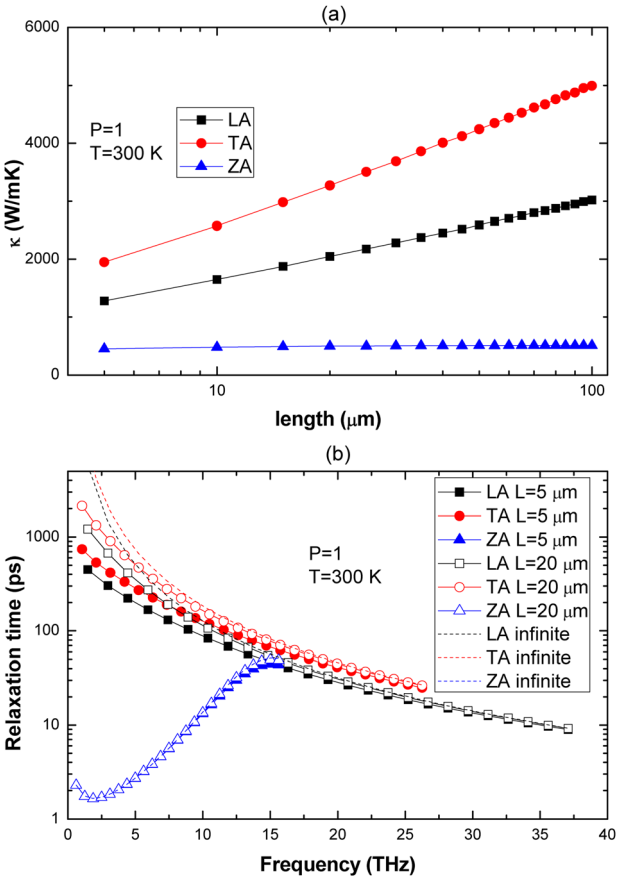

FIG. 3. (a) The length dependence of intrinsic thermal conductivity of LA, TA, and ZA branches in graphene ribbon. (b) The frequency dependence of relaxation time of LA, TA, and ZA phonons in graphene ribbons with different lengths.

with different length. Here the specularity parameter (P) is 1.0. The dashed lines indicate the relaxation time of phonons in infinite graphene sheet (no boundary scattering) according to Eqs. (6) and (12). The lines with solid symbols indicate the averaged relaxation time of phonons in 5 μm long graphene ribbon, and the lines with hollow symbols indicate that in 20 μm long graphene ribbon. In LA and TA branches, the relaxation time of phonons decreases sharply as the frequency of phonons increases. However, the frequency dependence is different in ZA branch. For ZA branch, the relaxation time is determined by the phonon group velocity and the Grüneissen parameter, thus it increases first, arrives its maximum value, then decreases with increasing frequency. In the case of $P = 1$ (specular boundary reflection), the relaxation time due to phonon-boundary scattering (τ_B) is only determined by the length of the ribbon. If the length is above micrometers, the relaxation time due to phonon-boundary scattering (τ_B) is significantly larger than that due to phonon-phonon Umklapp scattering (τ_U). According to the Matthiessen's rule $\tau^{-1} = \tau_U^{-1} + \tau_B^{-1}$, the length of the ribbon has weak effect on the phonon relaxation time, except for LA and TA phonons at low frequency region.

Fig. 4 shows the relative contribution of individual branch to thermal conductivity of graphene ribbons with different length at room temperature. Here, the width of ribbons is 1 μm and the specularity parameter is 0.8. In this case, TA branch has the maximal contribution because of the small Grüneissen parameter (1.0). The relative contribution of TA branch decreases with the length of the ribbon decreases; while the relative contribution of ZA branch increases as the length of the ribbon decreases. In the case of $L < 1$ μm, the contribution of ZA branch could be over 20%, therefore it is not negligible.

The diffuse phonon-boundary scattering suppresses the thermal conductivity of graphene ribbons. The MFP due to Umklapp phonon-phonon scattering of in-plane phonons is significantly longer than that of out-of-plane phonons, which is implied in Fig. 3(a). Therefore the suppression of thermal conductivity by the diffusive phonon-boundary scattering in LA and TA branches is more remarkable than that in ZA branch, which is clearly shown in Fig. 5(a). When the specularity parameter P decreases from 1 (purely specular reflection) to 0 (purely diffusive reflection), the thermal conductivity of LA (TA) branch decreases from 1643 W/mK to 950 W/mK (2582 W/mK to 1415 W/mK), while the contribution from ZA mode only decreases from 480 W/mK to 390 W/mK. The frequency dependence of the averaged relaxation time of LA, TA, and ZA phonons in graphene ribbons with different specularity parameters is shown in Fig. 5(b), which is helpful to understand the influence of the boundary scattering on the thermal conductivity of graphene ribbons. The width of the ribbon is 1 μm, and the length is 10 μm. The relaxation time of LA and TA branch phonons decreases as the specularity parameter decreases according to the Matthiessen's rule $\tau^{-1} = \tau_U^{-1} + \tau_B^{-1}$. Furthermore, because the relaxation time in the low-frequency regime is much longer than that in the high-frequency regime, the influence of the diffuse phonon-boundary scattering (or specularity parameter) on the relaxation time of LA and TA branch phonons is more significant in the low-frequency region. In ZA branch, the relaxation time of phonons in the high-frequency region decreases as the specularity parameter decreases, but the relaxation time of phonons at the low-frequency region does not change with the specularity parameter. For ZA phonons, due to the low phonon group velocity and the large absolute value of Grüneissen

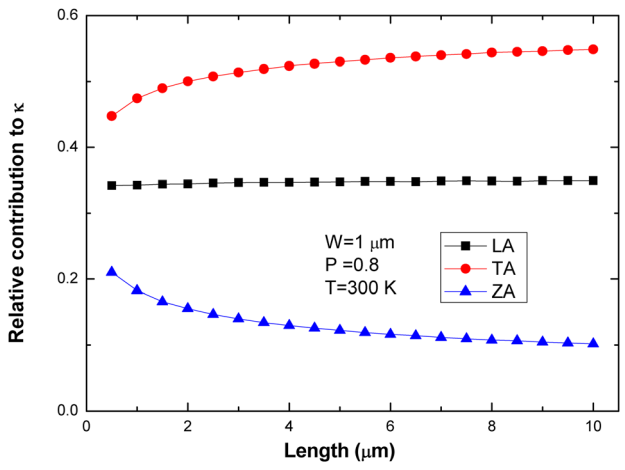

FIG. 4. The relative contributions from LA, TA, and ZA branches to the thermal conductivity as a function of the graphene ribbon length.

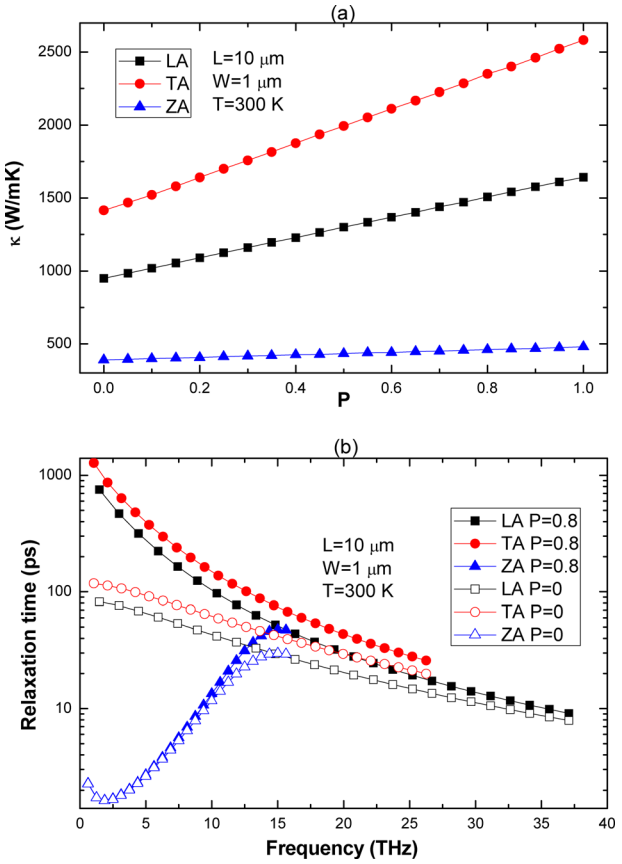

FIG. 5. (a) The thermal conductivity of LA, TA, and ZA branches at room temperature versus the specularity parameter. (b) The frequency dependence of relaxation time of LA, TA, and ZA phonons in graphene ribbon with different specularity parameters.

parameter (negative) at the low-frequency region, the phonon-phonon Umklapp scattering dominates over the phonon boundary scattering, this leads to the relaxation time of ZA phonons at the low-frequency region being insensitive on the specularity parameter.

Both Figs. 5(a) and 5(b) demonstrate that the influence of the specularity parameter on the thermal conductivity of ZA branch is much less than that of LA and TA branches, therefore the contribution of ZA mode to the thermal conductivity ($\frac{\kappa_{ZA}}{\kappa}$) increases as the specularity parameter decreases, which is shown in Fig. 6. It is also shown in Fig. 6 that the contribution of ZA branch to the thermal conductivity is dependent on the ribbon width. With the same specularity parameter, the contribution of ZA branch increases as the ribbon width decreases. The underlying reason is that when the ribbon width is smaller, the number of phonons that experience lateral boundary scattering is larger, thus the suppression of LA/TA branches is significantly stronger than that of ZA branch due to the huge difference in phonon relaxation time between the branches.

Fig. 7(a) gives the temperature dependence of thermal conductivity of individual phonon branch in a 10 μm long and 1 μm wide graphene ribbon. At high temperature, the thermal conductivities of LA, TA, and ZA branches approach a $1/T$ behavior, a characteristic of high temperature three-phonon scattering. At the low temperature limit, the thermal conductivity of LA and TA is proportional to T^2, but that of ZA is proportional to $T^{1.5}$, due to linear dispersion in LA and TA branch and quadratic dispersion in ZA branch. It is evident in Fig. 7(b) that the TA mode has the largest contribution to the thermal conductivity at room temperature, but the ZA mode is dominant at temperatures below 50 K. In the range from 0 to 100 K, the contribution of ZA decreases rapidly, while the contributions of in-plane branches increase rapidly. In the range above 200 K, the contribution of TA/LA increases/decreases slightly, while that of ZA has little change.

Fig. 8 gives the normalized accumulative distribution of thermal conductivity as a function of phonon frequency in LA, TA, and ZA branches at T = 300 K and T = 50 K, respectively. The normalized accumulative distribution of thermal conductivity is defined as $\frac{\kappa_\lambda(\omega)}{\kappa_\lambda}$, where $\kappa_\lambda(\omega)$ is the accumulative thermal conductivity of phonons with frequency from 0 to ω, which is derived as

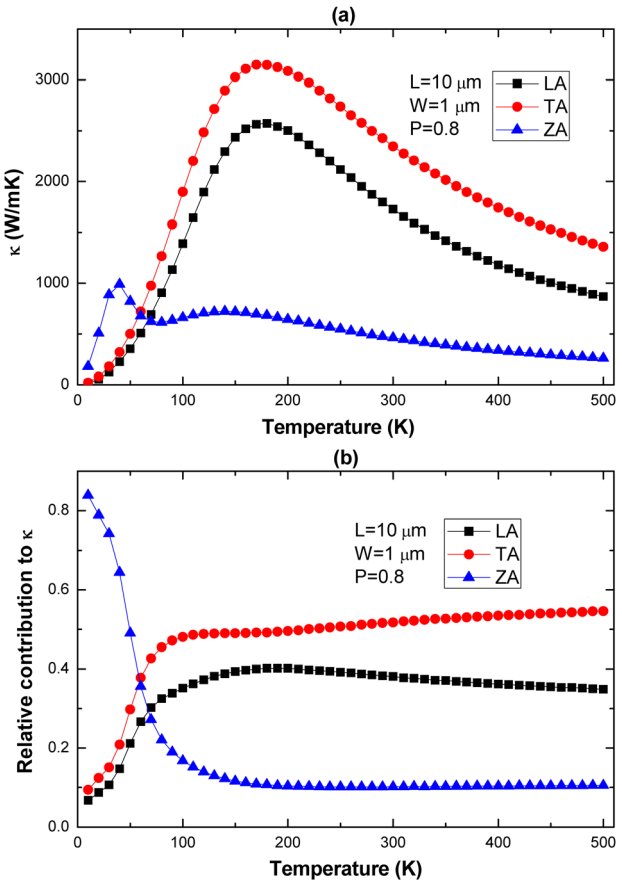

FIG. 7. (a) The temperature dependence of thermal conductivity of individual phonon branches in graphene ribbon. (b) The temperature-dependent relative contribution of individual phonon branches to the thermal conductivity of graphene ribbons.

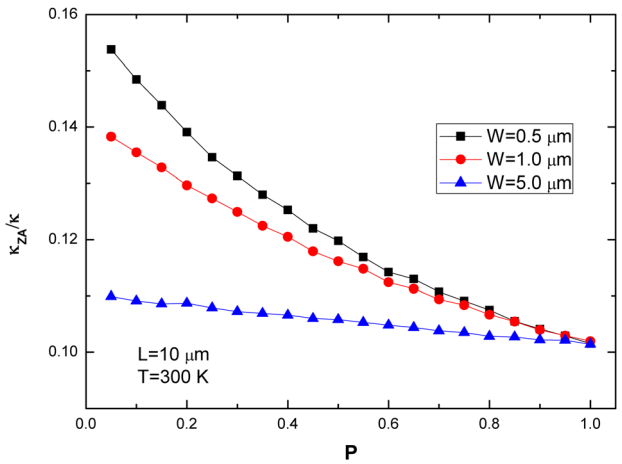

FIG. 6. The relative contribution of ZA branch to the thermal conductivity as a function of the specularity parameter at different graphene ribbon widths.

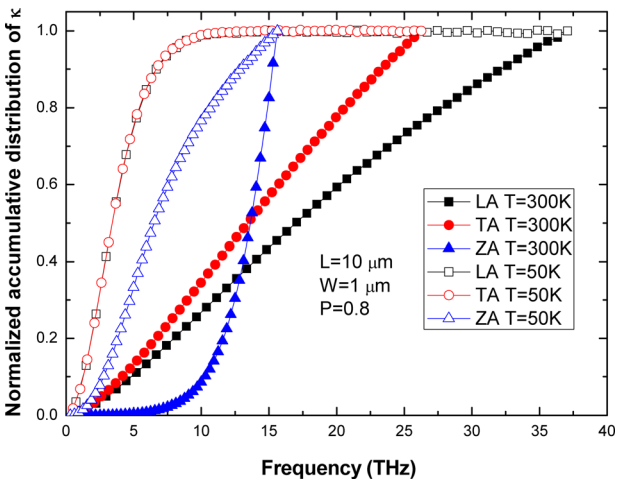

FIG. 8. The normalized accumulative distribution of thermal conductivity as a function of phonon frequency in LA, TA, and ZA branches at T = 300 K and T = 50 K.

$$\kappa_\lambda(\omega) = \begin{cases} \dfrac{k_B}{4\pi^2\delta}\displaystyle\int_0^{\omega}\int_0^{2\pi} \dfrac{(\hbar\omega/k_BT)^2 e^{\hbar\omega/k_BT}}{(e^{\hbar\omega/k_BT}-1)^2}\omega\cos^2\theta\tau_\lambda(\omega,\theta)d\theta d\omega & \lambda = LA,\ TA \\ \dfrac{k_B}{2\pi^2\delta}\displaystyle\int_0^{\omega}\int_0^{2\pi} \dfrac{(\hbar\omega/k_BT)^2 e^{\hbar\omega/k_BT}}{(e^{\hbar\omega/k_BT}-1)^2}\omega\cos^2\theta\tau_\lambda(\omega,\theta)d\theta d\omega & \lambda = ZA. \end{cases} \tag{16}$$

It is shown that at room temperature, near the first Brillouin zone center (low-frequency region), the value of $\frac{\kappa_\lambda(\omega)}{\kappa_\lambda}$ in ZA branch is much lower than that of LA and TA branches, but near the boundary of the first Brillouin zone (high-frequency region), it is remarkably higher than that of LA and TA branches because the group velocity and the Grüneissen parameter (negative) increase with the frequency in ZA branch. At T = 50 K, the contribution of high frequency phonons to the thermal conductivity decreases, especially in LA and TA branches, the phonons with frequency above 10 THz almost have no contribution to the thermal conductivity, because at low temperature, the number of high frequency phonons sharply decreases according to the Bose-Einstein distribution function. However, the group velocity and the Grüneissen parameter (negative) remarkably increase with the frequency in ZA branch, so the contribution of phonons near the boundary of the first Brillouin zone in ZA branch is much higher than that in LA and TA branches.

Above we have discussed the contributions of LA, TA, and ZA branches to thermal conductivity of graphene. Next, we explore the relative contribution of phonon branches with different models. We denote the model that includes the frequency dependent Grüneisen parameter and the special selection rule in ZA branch as model-1, which was adopted in the above calculation. This special selection rule[6,24] in ZA branch is obtained for flat graphene due to the reflection symmetry of ideal two-dimensional structure. However, in practical graphene devices, the geometry deformation[29–31] and substrate[32,33] will break this reflection symmetry, thus this selection rule is invalid. The second model (model-2) only considers the frequency dependence of Grüneisen parameter but does not include the special selection rule in ZA branch. As shown in Fig. 9, at room temperature (300 K), the contribution to the thermal conductivity by ZA branch in model-1 is 10.5%, while only 3.9% from model-2. This demonstrates that the relative contribution to thermal conductivity by ZA mode will be suppressed significantly in geometrically deformed graphene or in the supported graphene samples.

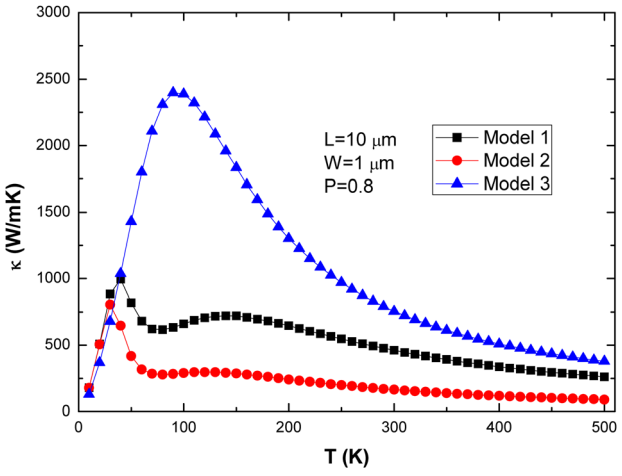

FIG. 9. The temperature dependence of thermal conductivity of ZA branch calculated using different models.

In the third model (model-3), the selection rule in ZA branch is not considered, and the Grüneissen parameter of ZA mode is set as a constant −1.5, which is adopted as the averaging of mode-dependent Grüneissen parameter over the relevant phonon wave-vector ranges in Ref. 34. As shown in Fig. 9, compared to the results from model-2 (3.9%), the contribution to the thermal conductivity by ZA branch in model-3 is 15.6% at 300 K. This demonstrates that the thermal conductivity of graphene is very sensitive to Grüneissen parameter. The frequency dependence of Grüneissen parameter in ZA branch is much stronger than that of LA and TA modes. From the first-principles calculations in Refs. 16 and 17, we suggest that the averaging of mode-dependent absolute value of Grüneissen parameter in ZA branch should be much larger than 1.5, so the contribution to the thermal conductivity by ZA branch in model-3 is overestimated.

IV. CONCLUSION

In this work, we have developed a general expression for the direction-dependent phonon-boundary scattering rate, and incorporated this general expression together with the special selection rule for three-phonon scattering of ZA phonons into the linearized Boltzmann transport equation in the relaxation time approximation. With this improved model, we have systematically investigated the effects of the size, boundary scattering and temperature of graphene ribbons on the relative contributions of thermal conductivity from LA, TA, and ZA branches. The results reveal that the size, boundary scattering mechanism, and temperature have different influences on the thermal conductivity of individual phonon branches due to the significant difference in the phonon dispersion between the in-plane and out-of-plane branches. The relative contribution of ZA branch to the thermal conductivity increases with decreasing the size, specularity parameter, and temperature of graphene ribbons. The contribution to the thermal conductivity by ZA phonons cannot be neglected, especially in the graphene ribbons with small size (less than 1 μm) and rough boundary (small specularity parameter). At temperature lower than 50 K, the contribution of ZA branch becomes dominant.

ACKNOWLEDGMENTS

This work was financially supported by National Natural Science Foundation of China (NSFC) (Grant Nos. 11275163, 11274011, 11204262, and 61274107), the Ministry of Education of China (Grant No. 20110001120133), the Hunan Provincial Natural Science Foundation of China (No. 13JJ4046), and the Scientific Research Fund of Hunan Provincial Education Department (No. 13B117).

[1]A. A. Balandin, S. Ghosh, W. Bao, I. Calizo, D. Teweldebrhan, F. Miao, and C. N. Lau, Nano Lett. **8**, 902 (2008).
[2]S. Ghosh, I. Calizo, D. Teweldebrhan, E. P. Pokatilov, D. L. Nika, A. A. Balandin, W. Bao, F. Miao, and C. N. Lau, Appl. Phys. Lett. **92**, 151911 (2008).
[3]Z. Wang, R. Xie, C. Bui, D. Liu, X. Ni, B. Li, and J. Thong, Nano Lett. **11**, 113 (2011).
[4]W. Cai, A. L. Moore, Y. Zhu, X. Li, S. Chen, L. Shi, and R. S. Ruoff, Nano Lett. **10**, 1645 (2010).
[5]S. Chen, A. L. Moore, W. W. Cai, J. Suk, J. An, C. Mishra, C. Amos, A. W. Magnuson, J. Y. Kang, L. Shi, and R. S. Ruoff, ACS Nano **5**, 321 (2011).
[6]J. H. Seol, I. Jo, A. L. Moore, L. Lindsay, Z. H. Aitken, M. T. Pettes, X. Li, Z. Yao, R. Huang, D. Broido, N. Mingo, R. S. Ruoff, and L. Shi, Science **328**, 213 (2010).
[7]D. L. Nika, S. Ghosh, E. P. Pokatilov, and A. A. Balandin, Appl. Phys. Lett. **94**, 203103 (2009).
[8]D. L. Nika, A. S. Askerov, and A. A. Balandin, Nano Lett. **12**, 3238 (2012).
[9]A. Bagri, S.-P. Kim, R. S. Ruoff, and V. B. Shenoy, Nano Lett. **11**, 3917 (2011).
[10]J. Lan, J. S. Wang, C. K. Gan, and S. K. Chin, Phys. Rev. B **79**, 115401 (2009).
[11]G. Zhang and H. Zhang, Nanoscale **3**, 4604 (2011).
[12]L. Lindsay, D. A. Broido, and N. Mingo, Phys. Rev. B **83**, 235428 (2011).
[13]T. Ouyang, Y. Chen, L.-M. Liu, Y. Xie, X. Wei, and J. Zhong, Phys. Rev. B **85**, 235436 (2012).
[14]A. Alofi and G. P. Srivastava, Phys. Rev. B **87**, 115421 (2013).
[15]D. L. Nika, E. P. Pokatilov, A. S. Askerov, and A. A. Balandin, Phys. Rev. B **79**, 155413 (2009).
[16]B. D. Kong, S. Paul, M. B. Nardelli, and K. W. Kim, Phys. Rev. B **80**, 033406 (2009).
[17]N. Mounet and N. Marzari, Phys. Rev. B **71**, 205214 (2005).
[18]E. Munoz, J. Lu, and B. I. Yakobson, Nano Lett. **10**, 1652 (2010).
[19]A. A. Balandin, Nature Mater. **10**, 569 (2011).
[20]D. L. Nika and A. A. Balandin, J. Phys.: Condens. Matter **24**, 233203 (2012).
[21]P. G. Klemens and D. F. Pedraza, Carbon **32**, 735 (1994).
[22]P. G. Klemens, J. Wide Bandgap Mater. **7**, 332 (2000).
[23]P. G. Klemens, Int. J. Thermophys. **22**, 265 (2001).
[24]L. Lindsay, D. A. Broido, and N. Mingo, Phys. Rev. B **82**, 115427 (2010).
[25]M. Roufosse and P. G. Klemens, Phys. Rev. B **7**, 5379 (1973).
[26]D. T. Morelli, J. P. Heremans, and G. A. Slack, Phys. Rev. B **66**, 195304 (2002).
[27]J.-W. Jiang, J.-S. Wang, and B. Li, Phys. Rev. B **79**, 205418 (2009).
[28]G. Xie, Y. Guo, B. Li, L. Yang, K. Zhang, M. Tang, and G. Zhang, Phys. Chem. Chem. Phys. **15**, 14647 (2013).
[29]V. B. Shenoy, C. D. Reddy, A. Rama, and Y. W. Zhang, Phys. Rev. Lett. **101**, 245501 (2008).
[30]V. B. Shenoy, C. D. Reddy, and Y. W. Zhang, ACS Nano **4**, 4840 (2010).
[31]C. Yu and G. Zhang, J. Appl. Phys. **113**, 044306 (2013).
[32]J. Chen, G. Zhang, and B. Li, Nanoscale **5**, 532 (2013).
[33]C. Yu and G. Zhang, J. Appl. Phys. **113**, 214304 (2013).
[34]Z. Aksamija and I. Knezevic, Appl. Phys. Lett. **98**, 141919 (2011).